Longitudinal Change Detected by Spectral Domain Optical Coherence Tomography in the Optic Nerve Head and Peripapillary Retina in Experimental Glaucoma

Nicholas G. Strouthidis,[1] *Brad Fortune,*[2] *Hongli Yang,*[1] *Ian A. Sigal,*[3] *and Claude F. Burgoyne*[1]

Purpose. To investigate whether longitudinal changes deep within the optic nerve head (ONH) are detectable by spectral domain optical coherence tomography (SDOCT) in experimental glaucoma (EG) and whether these changes are detectable at the onset of Heidelberg Retina Tomography (HRT; Heidelberg Engineering, Heidelberg, Germany)–defined surface topography depression.

Methods. Longitudinal SDOCT imaging (Spectralis; Heidelberg Engineering) was performed in both eyes of nine rhesus macaques every 1 to 3 weeks. One eye of each underwent trabecular laser-induced IOP elevation. Four masked operators delineated internal limiting membrane (ILM), retinal nerve fiber layer (RNFL), Bruch's membrane/retinal pigment epithelium (BM/RPE), neural canal opening (NCO), and anterior lamina cribrosa surface (ALCS) by using custom software. Longitudinal changes were assessed and compared between the EG and control (nonlasered) eyes at the onset of HRT-detected surface depression (follow-up 1; [FU1]) and at the most recent image (follow-up 2; [FU2]).

Results. Mean IOP in EG eyes was 7.1 to 24.6 mm Hg at FU1 and 13.5 to 31.9 mm Hg at FU2. In control eyes, the mean IOP was 7.2 to 12.6 mm Hg (FU1) and 8.9 to 16.0 mm Hg (FU2). At FU1, neuroretinal rim decreased and ALCS depth increased significantly (paired *t*-test, $P < 0.01$); no change in RNFL thickness was detected. At FU2, however, significant prelaminar tissue thinning, posterior displacement of NCO, and RNFL thinning were observed.

Conclusions. Longitudinal SDOCT imaging can detect deep ONH changes in EG eyes, the earliest of which are present at the onset of HRT-detected ONH surface height depression. These parameters represent realistic targets for SDOCT detection of glaucomatous progression in human subjects. (*Invest Ophthalmol Vis Sci.* 2011;52:1206–1219) DOI:10.1167/iovs.10-5599

Glaucoma is recognized as a progressive optic neuropathy, therefore accurate characterization of changes at the optic nerve head (ONH) as well as at the retinal nerve fiber layer (RNFL) is of central importance in the management of glaucoma. Although evaluation of the ONH and RNFL by stereoscopic ophthalmoscopy remains the mainstay of clinical assessment, a role for semiautomated imaging devices has been increasingly recognized. Although much emphasis has been placed on using such devices to assist the clinician in discriminating between a normal optic disc and an abnormal or glaucomatous disc at presentation, a perhaps more useful application lies in their ability to detect longitudinal change. To date, most longitudinal imaging studies have used confocal scanning laser tomography (CSLT), in particular, the Heidelberg Retina Tomograph (HRT, Heidelberg Engineering, Heidelberg, Germany), either by measuring changes in surface height (topographical change analysis [TCA]) or changes in the neuroretinal rim area.[1–3] Progressive nerve fiber layer loss has also been reported in glaucoma subjects based on measurements by time domain optical coherence tomography (TDOCT),[4,5] and more recently, longitudinal RNFL changes have been documented by scanning laser polarimetry (SLP).[6] It should be noted, however, that the preponderance of longitudinal imaging studies using the CSLT, as opposed to other imaging modalities, reflects the length of time CSLT has been available compared with newer techniques. This remains a central problem; as development and improvement in imaging hardware and software tend to occur at a more rapid rate than the evaluation of their ability to detect longitudinal change.

One approach, which may help establish a new device's ability to detect longitudinal change, is the use of an experimental glaucoma (EG) model. In the case of the nonhuman primate model, the experimental neuropathy is largely clinically indistinguishable from that observed in human glaucoma, and the changes observed develop over the course of months rather than years or decades, as in humans. The ONH of the rhesus macaque has an anatomy similar to that of the human, in particular the presence of a connective tissue lamina cribrosa. In our laboratory, we have used these anatomic similarities to explore structural changes at the earliest stages of EG optic neuropathy using postmortem 3D histomorphometric ONH reconstructions.[7,8] Our postmortem studies suggest that the structural ONH abnormalities occurring at the earliest stages of the experimental neuropathy include posterior displacement of the lamina cribrosa, thickening of the lamina cribrosa, a widening of the scleral canal opening, and a thick-

From the [1]Optic Nerve Head Research Laboratory, [2]Discoveries in Sight Laboratories, and the [3]Ocular Biomechanics Laboratory, Devers Eye Institute, Legacy Health, Portland, Oregon.

Supported by Grant R01-EY11610 from the National Institutes of Health, Legacy Good Samaritan Foundation, Heidelberg Engineering, and Sears Medical Trust. NGS was funded by an unrestricted grant from Heidelberg Engineering and by a Royal College of Ophthalmologists/Pfizer Fellowship.

Submitted for publication March 26, 2010; revised June 15 and September 20, 2010; accepted November 1, 2010.

Disclosure: **N.G. Strouthidis**, Heidelberg Engineering (F, R); **B. Fortune**, Heidelberg Engineering (F); **H. Yang**, None; **I.A. Sigal**, None; **C.F. Burgoyne**, Heidelberg Engineering (F, R)

Corresponding author: Claude F. Burgoyne, Optic Nerve Head Research Laboratory, Devers Eye Institute, Legacy Health System, 1225 NE Second Avenue, PO Box 3950, Portland, OR 97208-3950; cfburgoyne@deverseye.org.

ening of the prelaminar tissue.[7–9] We believe that these changes may well represent the earliest signs of an ONH in distress from an IOP-related insult, which would make them an important target for detection by in vivo imaging. These anatomic targets, deep from the surface of the cup, are theoretically within the resolution of spectral domain optical coherence tomography (SDOCT). Indeed, one recent report of a cross-sectional examination of a cohort of glaucomatous and ocular hypertensive eyes suggested that the full width of the lamina cribrosa can be detected in human subjects by 3D SDOCT imaging and that thinning of the lamina cribrosa correlates with the decrease in visual field mean deviation.[10]

The purpose of this study was therefore to investigate whether longitudinal changes deep within the ONH, as well as RNFL and neuroretinal rim changes, are detectable by longitudinal SDOCT imaging in an experimental model of glaucomatous optic neuropathy. We also sought to determine whether deep ONH changes are detectable by SDOCT at the onset of change in ONH surface topography, as detected by CSLT.

Methods

Animal Selection

The local Institutional Animal Care and Use Committee (Legacy Health) approved this study, and all animals were treated in accordance with the ARVO Statement for the Use of Animals in Ophthalmic and Vision Research. Nine adult rhesus macaque monkeys (*Macaca mulatta*) were included in this study.

Imaging Protocol

The ophthalmic imaging procedure began with induction of general anesthesia by veterinary staff (Legacy Health) using ketamine (15 mg/kg, by intramuscular injection) and midazolam (0.2 mg/kg, by intramuscular injection). A single SC injection of atropine sulfate (0.05 mg/kg) was also administered. The animals were then intubated with an endotracheal tube. An intravenous (IV) line (24-gauge, 0.75-in.; Insyte Autoguard IV Catheter; BD Biosciences, Franklin Lakes, NJ) was then placed into the saphenous vein to administer fluids (lactated Ringer's solution, 10 mL/kg/h and/or 6% hetastarch) for maintenance of hydration and normal blood pressure. One drop of topical corneal anesthetic was placed in each eye (0.5% proparacaine), and a lid speculum was inserted to keep eyelids open. Intraocular pressure (IOP) was measured by applanation tonometry (Tonopen XL; Reichert, Depew, NY) and reported as the average of three or more measurements at each session. The endotracheal tube was connected to an anesthesia machine and animals began breathing a mixture of 100% oxygen and isoflurane gas (1%–2%; typically, 1.25%) to maintain anesthesia for the duration of the imaging session. Pupillary dilation was induced topically with one drop each of tropicamide (0.5%) and phenylephrine (2.5%) in each eye. A clear, plano-powered, rigid, gas-permeable contact lens was placed on each eye with topical lubricant (0.5% carboxymethylcellulose sodium; Refresh; Allergan, Irvine, CA). Heart rate and arterial oxyhemoglobin saturation were monitored continuously throughout each session (Propaq Encore model 206EL; Protocol Systems, Inc., Beaverton, OR) and maintained above 75 per minute and 95%, respectively. Body temperature was maintained at 37°C with a pair of warm-water heating pads (TP500 T/Pump; Gaymar Industries, Orchard Park, NY) placed above and below the animal. Blood pressure was measured approximately every 10 minutes (NIBP system 7100; Advanced Medical Instruments, Inc., Broken Arrow, OK) and maintained above a mean arterial pressure (MAP) of 75 mm Hg. If MAP decreased below 70 mm Hg, an IV bolus of lactated Ringer's (10 mL/kg) was delivered over 3 to 5 minutes and repeated if necessary after 10 minutes. Before imaging commenced, the intraocular pressure was adjusted to 10 mm Hg by using a manometer connected to a 27-gauge cannula, which was inserted through the temporal cornea into the anterior chamber. Imaging began after 30 minutes of IOP stabilization at 10 mm Hg.

All SDOCT imaging was performed with a commercially available device (Spectralis; Heidelberg Engineering GmbH, Heidelberg, Germany). For this study, an 80 radial B-scan pattern was acquired over a 15° area (768 A-scans per B-scan). All image acquisitions were centered on the ONH, and this scan location was consistent in all images used in this study. The device's eye tracking facility was turned on during image acquisition to enable B-scan acquisition repetition ($n = 9$) and sweep-averaging in real time to reduce speckle noise. For each eye, at each imaging session, the 80 B-scans were acquired relative to a single reference image. Therefore, for each eye, the location of each B-scan remained stable within all pre- and postlaser images.

Both eyes of each animal underwent baseline imaging on three to four occasions before the commencement of argon laser treatment of the trabecular meshwork of one eye to induce unilateral, chronic, mild-to-moderate IOP elevation. Laser treatment was repeated approximately every 2 weeks to induce a sustained elevation in IOP. The eye in which laser treatment was performed will hereafter be referred to as the EG eye and the untreated fellow eye as the control eye. Imaging of both eyes of each animal continued every 2 to 3 weeks after the commencement of laser therapy.

In addition to SDOCT imaging with Spectralis (Heidelberg Engineering), CSLT images were also acquired from both eyes at each imaging session using the HRT II. Two measures of HRT II-defined surface height depression (assumed to be posterior deformation) were used to identify the onset of EG optic neuropathy. The first of these methods, used the parameter mean position of the disc (MPD), which is described in other publications.[11,12] Briefly, MPD refers to the height of the surface of the ONH (i.e., average of all pixels located within the contour line) relative to the height of a reference located on the peripapillary surface. $MPD_{Baseline}$ was calculated for each eye as the mean MPD from all prelaser baseline images. MPD onset was defined as the first postlaser session when MPD exceeded the 95% confidence limits of the $MPD_{Baseline}$ for that eye, if the change was confirmed in two subsequent follow-up imaging sessions. The second method used was topographical change analysis (TCA), the native progression algorithm contained within the HRT II Explorer software platform (Artes PH, et al. *IOVS* 2006;47:ARVO E-Abstract 4349).[1,13] TCA onset was defined as the first session when 20 or more significantly depressed superpixels were present within the disc margin, confirmed in two subsequent sessions.

For the purposes of this study, four time points were selected for each animal, from which a single SDOCT volume from each eye at each time point was analyzed. Two baseline time points, baseline 1 (BL1) and baseline 2 (BL2), were selected randomly from the series of three or four prelaser imaging sessions. Two follow-up time points were selected from the sequence of sessions beginning after the onset of laser treatment. The first follow-up SDOCT volume, follow-up 1 (FU1), was chosen to be the time point when CSLT-defined surface height depression was first identified, either by MPD change or by TCA change, whichever occurred first. The second follow-up SDOCT volume, follow-up 2 (FU2) was chosen from the most recently available imaging session for each animal. This approach was taken to ensure that the EG eyes could be expected to be homogenous in terms of early experimental damage at FU1, but heterogeneous in terms of the stage of damage at FU2. Furthermore, it enabled us to determine whether any of the deep ONH changes identified at later stages of glaucomatous optic neuropathy would manifest at the onset of CSLT-detected ONH surface height depression.

Delineation and Parameterization of SDOCT Volumes

Most of the SDOCT delineation methodology used in this study has been described in detail elsewhere.[14,15] Briefly, the raw SDOCT data from each volume was exported into a custom-built, 3D visualization and delineation software (Multiview, based on the Visualization Tool-

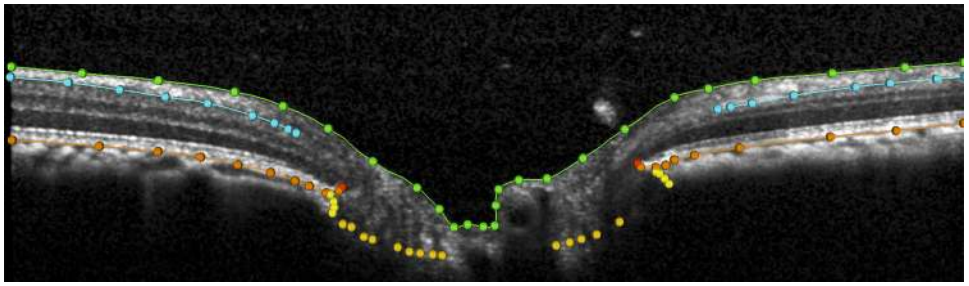

FIGURE 1. Delineation of landmarks within an ONH SDOCT B-scan. *Green*: ILM; *blue*: posterior surface of RNFL; *orange*: posterior surface of RPE/BM complex; *red*: NCO, located at the innermost termination of the RPE/BM complex; *yellow*: BT of Elschnig, located at the innermost termination of choroidal signal; *gold*, ALCS. See Figure 2 for description of how this structure was identified.

kit; VTK, Clifton Park, NY). Four observers, masked to both eye status (whether EG or control) and time point, manually delineated pertinent features within alternating B-scans in each SDOCT volume (i.e., 40 B-scans per 80 radial B-scan volume, with the first delineated B-scan being at the vertical, 0° location). The features delineated were the internal limiting membrane (ILM), posterior surface of the RNFL, the posterior surface of the Bruch's membrane/retinal pigment epithelium complex (BM/RPE), the neural canal opening (NCO; located on either side of the neural canal at the innermost termination of the BM/RPE),[14] border tissue (BT) of Elschnig (located on either side of the neural canal at the innermost termination of the choroidal signal),[16] and the anterior lamina cribrosa surface (ALCS). An example of the B-scan with the delineation categories is provided in Figure 1.

In the case of the ILM, RNFL, BM/RPE, and BT categories, each surface was delineated using discrete points interconnected by a Bézier curve. The position of each point in each category was finely adjusted so that the fitted Bézier curve matched the feature of interest as closely as possible. The NCO was delineated using two discrete points at either side of the neural canal in each B-scan.[14] Our strategy for identifying the ALCS was based on our previous direct comparisons between SDOCT B-scans and matched histologic sections obtained from the same normal monkey eye.[17] We identified the ALCS as being the point where horizontal high-intensity signal below the disc surface begins to intersect the high-intensity vertical striations, which we identified as the prelaminar glial columns (Fig. 2).[17] It is important to note that the signal from the ALCS may be discontinuous in regions where there is pronounced shadowing caused by overlying retinal vessels. It is for this reason that the ALCS was delineated using discrete marks, rather than continuous Bézier curves. The observer could employ any number of marks, at their discretion, to delineate the ALCS.

All x,y dimensions in the SDOCT volumes were rescaled from the linear units reported by the Spectralis (which assumes human eye optics and dimensions) to estimates optimized for the monkey eye using a scaling factor of 0.857, which was based on the average axial length of 20.6 mm obtained from measurements on 16 of the 18 eyes in this study. Structural parameters were based on these scaled delineations (MatLab; The MathWorks, Natick, MA). Two reference planes were used for quantification purposes. The best-fitting ellipse through the 80 delineated NCO points in each volume defined the primary reference plane.[14,16] A secondary reference plane was based on a peripheral location along the RPE/BM complex, 1500 μm external to the NCO centroid.[15] The depth of the NCO centroid relative to the secondary, peripheral reference plane was calculated for each eye (Fig. 3A). RNFL thickness (RNFLT) was calculated at an eccentricity of 1200 μm from the NCO centroid (Fig. 3B) as previously described.[15] The RNFL volume (RNFLV) represents the volume of RNFL between the eccentricities of 1200 and 1500 μm from the NCO centroid. It is bounded above and below by the ILM and RNFL surfaces, respectively, interpolated across all 40 B-scans, internally by a cylinder with a 1200-μm radius oriented perpendicular to the NCO plane and externally by a cylinder with a 1500-μm radius oriented perpendicular to the NCO plane (Fig. 3C). The NCO area was calculated as the area of the best-fitting ellipse determined by the 80 delineated NCO points.[14] Likewise, the BT area was calculated as the area of the ellipse determined by the innermost delineated BT point at either side of the neural canal in each of the 40 B-scans (Fig. 3D). The neuroretinal mean rim width was calculated as the shortest distance between the NCO and the ILM (Fig. 4A), and the neuroretinal rim volume was calculated as the volume anterior to the NCO reference plane, contained by the ILM and a vertical perpendicular projection from the NCO (Fig. 4B). Most of these parameters are reported as the mean of the 80 samples obtained in each SDOCT volume (such as mean RNFLT and mean rim width); however, the rim volume parameter represents the sum of the 80 samples in each volume (Fig. 4B) and the two area measurements (NCO and BT) represent the area of the best-fitted ellipse, as described.

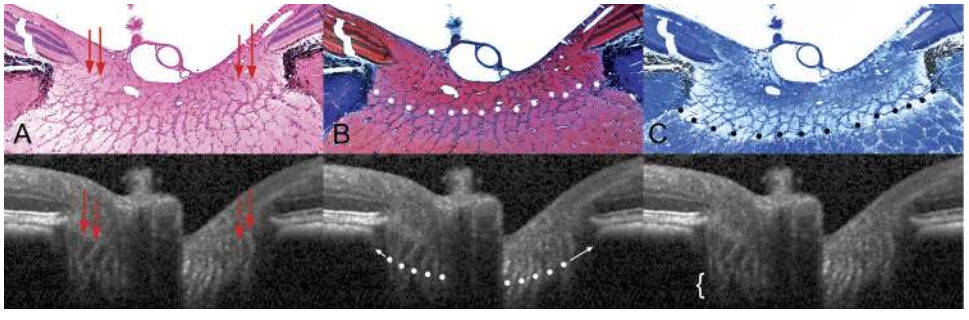

FIGURE 2. Detection of lamina cribrosa by SDOCT. Horizontal B-scans acquired at IOP 10 mm Hg from a normal monkey ONH were compared with matched histologic sections through the same ONH, perfusion fixed at IOP 10 mm Hg. (**A**) Prelaminar glial columns correspond to vertical striations seen in the matched interpolated B-scan below (*red arrows*). Hematoxylin and eosin. (**B**) The anterior lamina surface is delineated with *white glyphs.* Note that the peripheral insertion of the lamina is not clearly visible in the interpolated B-scan, although the approximate level of insertion may be ascertained by following the contour of the anterior laminar signal to the periphery of the neural canal (*white arrows*). The masked observers delineated the anterior laminar surface as the region where horizontal reflectance signals begin to interconnect the vertical striated signals, equivalent to the point where horizontal connective tissue beams begin to interconnect the base of the prelaminar glial columns. Masson trichrome. (**C**) The posterior lamina surface is delineated with *black glyphs* in the histologic section. The posterior surface is not detectable in the matched interpolated B-scan, as the signal fades rather than comes to a discrete termination (*white bracket*). The masked observers therefore did not delineate the posterior laminar surface. Luxol fast blue. (**A–C**) Magnification, ×10. Figure previously published in Strouthidis NG, Grimm J, Williams GA, Cull GA, Wilson DJ, Burgoyne CF. A comparison of ONH morphology viewed by spectral domain optical coherence tomography and by serial histology. *Invest Ophthalmol Vis Sci.* 2010;51:1464–1474. © ARVO.

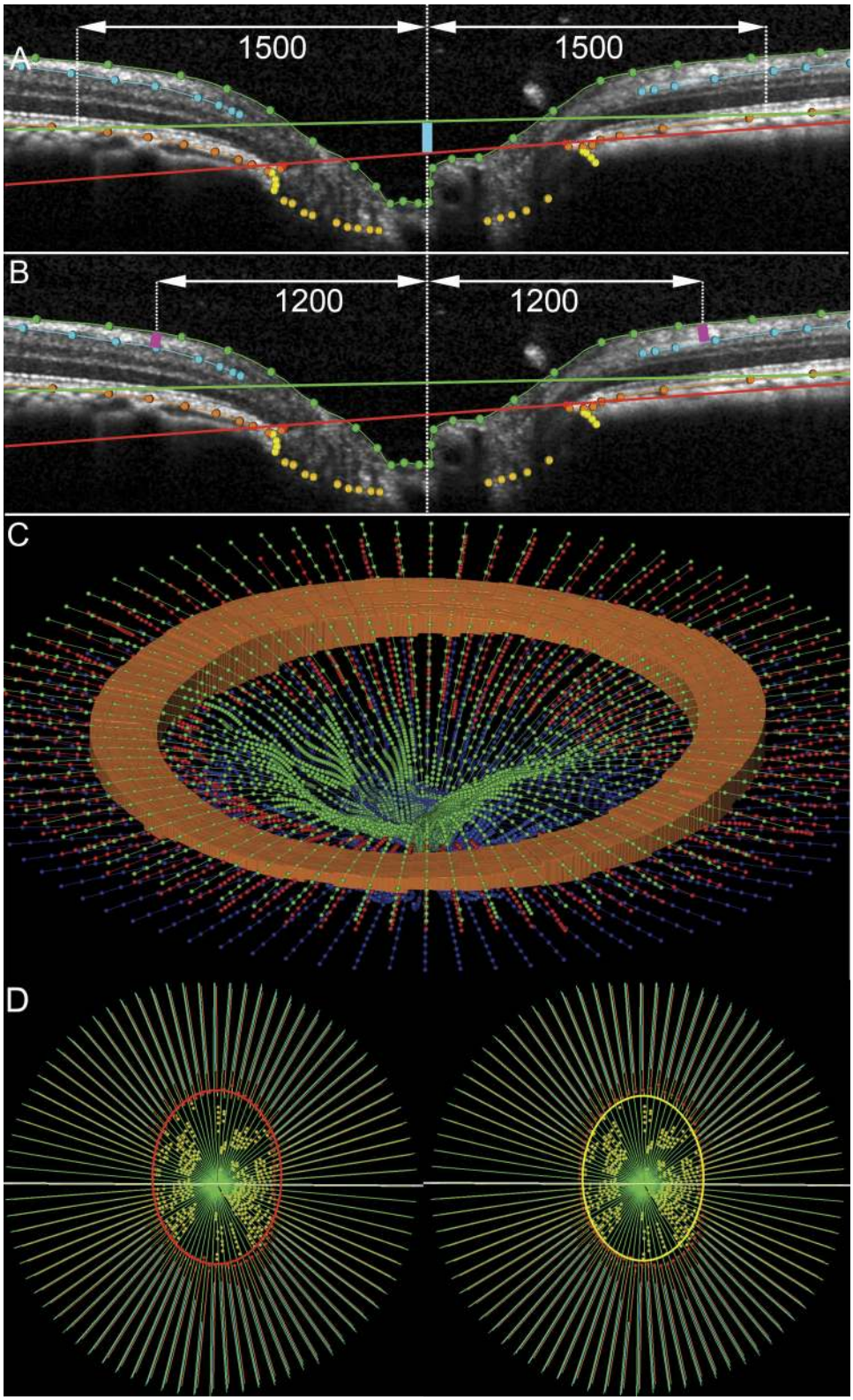

FIGURE 3. Parameterization of spectral domain optical coherence tomography volumes. (**A**) A horizontal B-scan. The primary reference plane (*red line*) is located at the level of the NCO. A secondary, peripheral reference plane is located at Bruch's membrane at 1500 μm eccentricity from the NCO centroid. The mean depth of the NCO is measured from the secondary reference plane to the NCO (*turquoise line*). (**B**) Mean RNFLT is measured between the ILM and the posterior surface of the RNFL at 1200-μm eccentricity from the NCO centroid (*pink lines*). (**C**) Three dimensional view to illustrate the RNFLV, shown as an orange circumpapillary cylinder bound by the internal limiting membrane (*green*) between 1200 and 1500 μm eccentricity from the NCO centroid and the posterior surface of the RNFL (in this panel shown here in *red* and in **A** and **B** in turquoise). (**D**) The en face view of a fully delineated volume is shown. *Left*: the *red ellipse* defines the NCO area. *Right*: BT area is bound by the *yellow ellipse*, located at the innermost BT delineations.

In terms of parameters involving the ALCS delineations, several measures were undertaken to account for varying completeness of the delineated surface (primarily because of vessel shadowing) and various densities of ALCS points made on each volume. First, only laminar points from sectors that were shared between all four SDOCT volumes for a given eye were used in the analysis. In other words, the analysis only considered regions of the lamina that were delineated in all four SDOCT volumes. The analysis was achieved as follows: all initially delineated ALCS marks were projected onto the NCO ellipse plane. The ellipse was then converted to unit circle space and the area bound within, containing each of the laminar points, divided into a grid of 100 equal area sectors using concentric rings and radial lines (Fig. 5). If two or more lamina points were contained within one of these sectors in all four images, then the points contained within that sector were in-

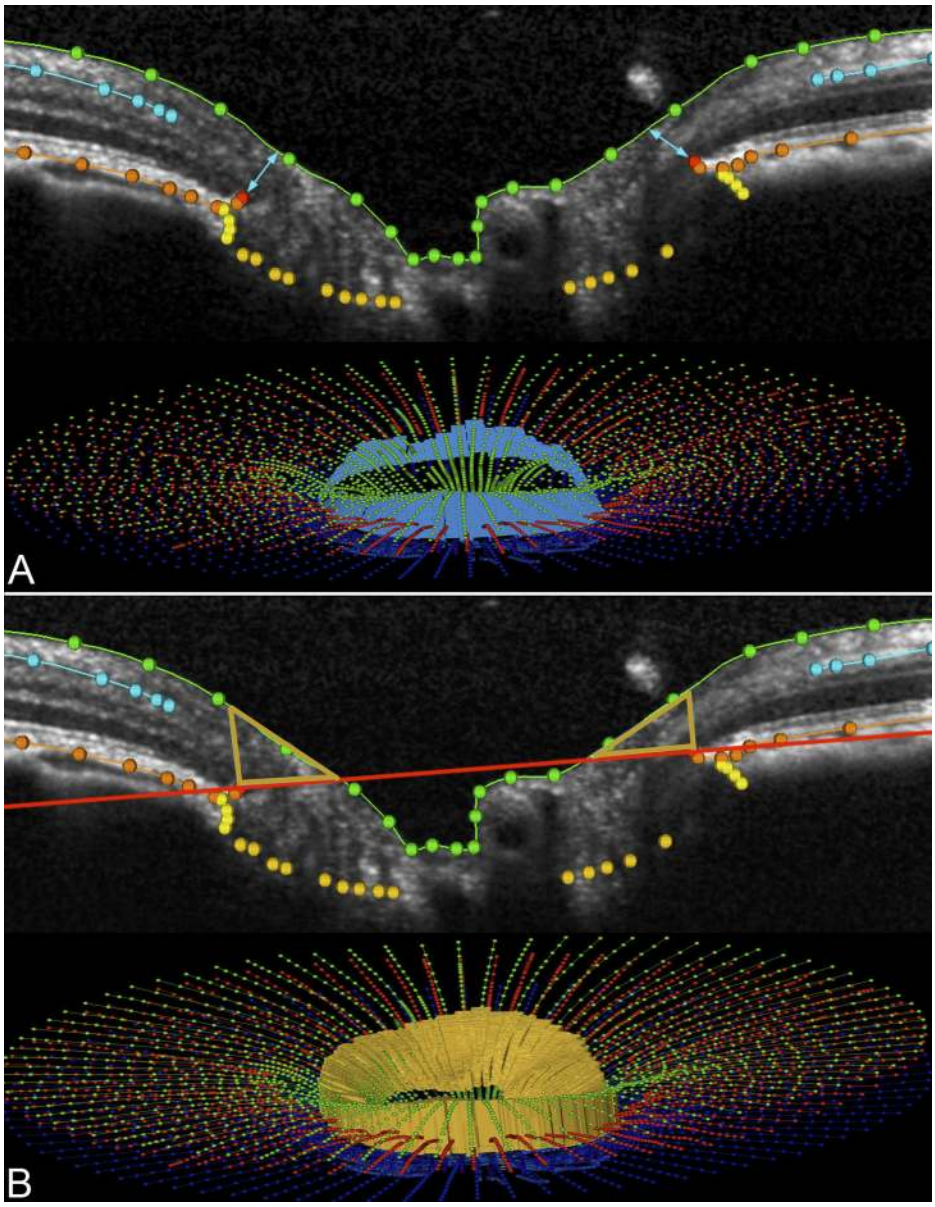

FIGURE 4. Generation of neuroretinal rim parameters in an SDOCT ONH volume. (**A**) Mean rim width is derived from the minimum distance from the NCO to the ILM (*turquoise arrows* in the upper B-scan). A three-dimensional representation of mean rim width is shown in a fully delineated volume (*turquoise band* in the lower image). (**B**) Mean rim volume is generated from the volume bound between the NCO and the ILM, shown in two dimensions by *gold triangles* in a horizontal B-scan (*top*) and in three dimensions (*gold*, *bottom*).

cluded in the analysis. If fewer than two points were contained in all four images, then the points contained within the sector were excluded from the analysis. After this point-filtration method, the circle space was converted back to the original ellipse configuration. This process is illustrated in Figure 5.

Second, the delineated ALCS points were weighted, so that points in the peripheral lamina contributed greater weight to the mean than those in the central portion of the lamina. The reason for the weighting was that the points in the peripheral part of the lamina represent a wider arc than those toward the center of the lamina (i.e., the area of the ALCS wedge represented by a given point increases with the distance that point is from the center of the lamina). The weightings for each delineated point were thus proportional to the distance from the NCO centroid.

Using the shared set of weighted ALCS points, we calculated prelaminar tissue thickness (PLTT) and anterior laminar cribrosa depth (ALCS depth). PLTT was calculated in 3D as the distance between the ALCS and the ILM, measured along the normal to the tangent of the local ALCS. The mean PLTT was calculated for all shared ALCS points in each volume. ALCS depth was calculated as the mean distance from the ALCS to the NCO reference plane (ALCS $\text{depth}_{\text{NCO}}$) and also as the mean distance to the peripheral BM/RPE reference plane (ALCS depth_{BM}), along the normal to each plane, respectively. Methods for quantifying these three parameters related to the ALCS are illustrated in Figure 6.

Statistical Analyses

The effects of treatment (EG versus control), time, and the treatment–time interaction were assessed for each structural parameter using repeated-measures analysis of variance (RM-ANOVA) matched for animal (EG eye matched to fellow control eye for each animal). Significant parameter change within individual eyes was identified by establishing a threshold criterion for change based on the coefficient of repeatability (RC) for each parameter.[18] The RC for each parameter was estimated from the two baseline measurements (BL1 and BL2) in each cohort of eyes. As 95% of repeated measurements are expected to be within the range of the RC, any difference from the average baseline to FU1 or FU2 that exceeded the RC was flagged as significant change rather than as being within the range of measurement error. The proportion of EG eyes identified as significantly changing could be regarded as positive hit rate, a proxy measure of sensitivity. The

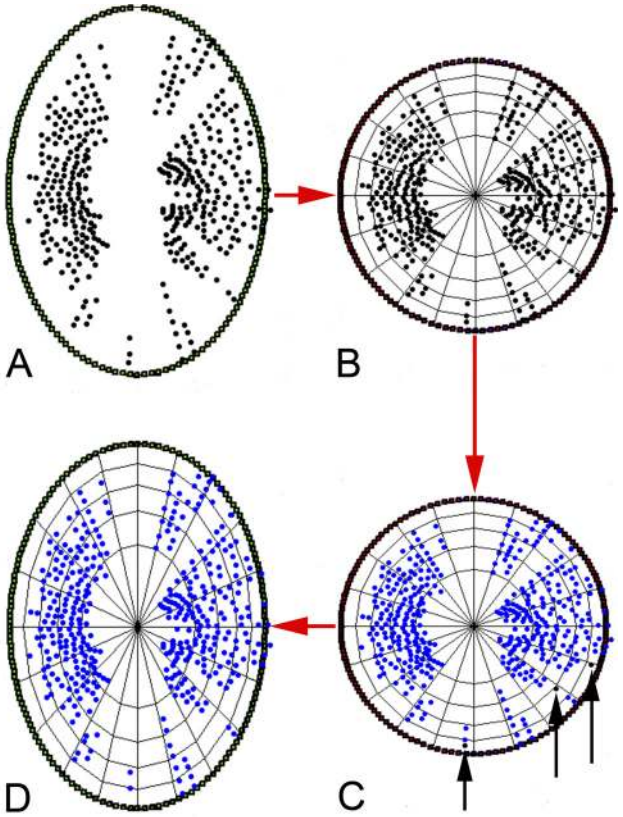

FIGURE 5. Method of ALCS point filtration. (**A**) The ALCS points (*black glyphs*) are projected onto the plane of an ellipse best fit to the NCO delineations (*green glyphs*). (**B**) The NCO ellipse is scaled into unit circle space and subdivided into 100 regions of equal area. (**C**) Regions where two or more ALCS-delineated points are present in all four volumes in the sequence are maintained for analysis as shared regions. Regions where there are fewer than two delineated points (*black glyphs*, highlighted by *black arrows*) common to all four volumes in the sequence are filtered out of the analysis. (**D**) The circle is transformed back to elliptical space, with the shared ALCS points shown.

number of control eyes flagged as changing could be regarded as a measure of the false-positive rate, and therefore as a proxy measure of specificity. The 95% confidence intervals (CIs) were calculated according to standard methods (Wilson interval for binomial proportions); comparisons of proportions for the positive hit rate at each follow-up time point were made between treated and control eye groups using the *Z*-test for two proportions (statistical analyses performed with Prism ver. 4.0; GraphPad Software, Inc., San Diego, CA, or Excel; Microsoft Corp., Redmond, WA).

RESULTS

The mean age of animals was 11 years (range, 9–19) and the mean length of follow-up after initiation of laser treatments until FU1 was 2.8 months (range, 1.2–5.8) and until FU2 was 10.7 months (range, 7.1–14.0). Mean postlaser IOP in the group of EG eyes ranged from 7.1 to 24.6 mm Hg at FU1 and from 13.5 to 31.9 mm Hg at FU2. Over the same period in the group of control eyes, the mean IOP ranges were 7.2 to 12.6 mm Hg (FU1) and 8.9 to 16.0 mm Hg (FU2). The peak IOP range in the EG eyes was 11.7 to 32.7 mm Hg (FU1) and 23.7 to 61.0 (FU2); for the control eyes the peak IOP range was 10.3 to 17.7 mm Hg (FU1) and 15.0 to 22.3 (FU2). The cumulative IOP difference was used to estimate the total postlaser IOP insult sustained by each EG eye compared with its fellow control eye. For each EG eye, the IOP difference from the fellow control eye was multiplied by the number of days from the last measurement and summed over the period of postlaser follow-up (IOP difference $\times$ days). The cumulative IOP difference ranged from -68.2 to 325.7 mm Hg-days at FU1 and from 788.7 to 5755.8 mm Hg-days at FU2. The IOP data and demographics of the monkeys included in the study are summarized in Table 1.

The distribution of parameter values at each time point, for both the group of EG eyes and the group of control eyes, is shown in Figure 7. Statistical analysis (RM-ANOVA) identified a significant effect of treatment and a significant time–treatment interaction for the following parameters: ALCS $\text{depth}_{\text{NCO}}$ (Fig. 7A), ALCS depth_{BM} (Fig. 7B), NCO depth (Fig. 7C), RNFLT (Fig. 7D), mean rim width (Fig. 7E), rim volume (Fig. 7F), and PLTT (Fig. 7G). When post hoc testing was applied to these parameters, a significant difference between the group of EG eyes and the group of their fellow control eyes was found at FU2 ($P < 0.001$ for each of the seven parameters). There was no significant effect of treatment nor a treatment–time interaction found for NCO area (Fig. 7H) or BT area (Fig. 7I). Though the distribution of parameter values for the group of EG eyes suggests that the EG eyes exhibited an increase in ALCS $\text{depth}_{\text{NCO}}$ (Fig. 7A), ALCS depth_{BM} (Fig. 7B), and NCO

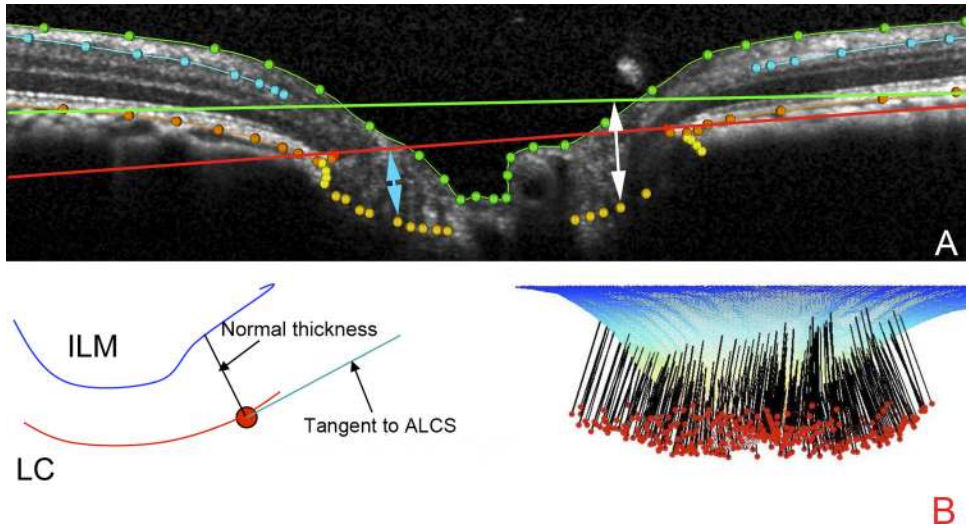

FIGURE 6. Parameters derived from the ALCS delineations. (**A**) ALCS depth is the perpendicular distance from the NCO reference plane to the ALCS $\text{depth}_{\text{NCO}}$, (*turquoise arrow*). A secondary ALCS depth is the perpendicular distance from the Bruch's membrane reference plane to the ALCS (ALCS depth_{BM}). (**B**) *Left*: the PLTT is measured as the normal from the tangent to the ALCS to the ILM. *Right*: PLTT measurement normals for a full 3D volume.

Table 1. Demographics and IOP Characteristics of Animals Included in the Study

Subject	Sex	Age (y)	Weight (kg)	Time after Laser (mo) FU1/FU2	Mean IOP EG FU1/FU2*	Mean IOP Control FU1/FU2*	Peak IOP EG FU1/FU2*	Peak IOP Control FU1/FU2*	Cumulative IOP Difference FU1/FU2*
135	M	11	13.2	1.5/7.3	10.8/14.6	9.8/11.1	13.0/40.3	12.3/18.7	41.7/839.0
137	M	10	13.0	1.8/7.1	24.6/31.9	12.4/16.0	29.7/49.0	17.7/22.3	233.7/3861.0
18389	F	19	8.8	2.5/8.3	7.1/14.4	7.2/8.9	14.3/39.0	10.3/18.0	53.7/1698.0
20377	F	10	5.4	3.6/12.2	11.2/23.9	9.2/10.6	17.0/52.0	12.7/19.0	319.7/5468.7
20655	F	10	8.4	5.8/14.0	11.4/13.5	9.9/11.5	16.7/23.7	15.0/15.0	60.0/788.7
21075	M	9	13.1	3.5/12.8	10.1/26.1	10.1/10.9	11.7/61.0	15.0/15.0	−68.2/5755.8
21152	F	9	7.1	2.2/7.9	22.0/27.3	12.6/11.0	27.3/49.7	13.7/15.0	298.3/4081.9
21808	F	9	6.5	1.2/13.8	21.4/20.8	12.1/12.3	32.7/34.3	13.7/16.7	325.7/4029.7
23534	F	11	4.5	3.6/12.9	10.6/19.6	11.0/10.8	16.7/36.3	14.0/15.7	19.7/3610.7

* Mean mm Hg (SD).

depth (Fig. 7C) at FU1, there were no significant differences found by post hoc testing between the EG and control eye groups at FU1. The results of the two intraeye longitudinal change analyses described below, however, suggest that the cross-sectional analysis shown in Figure 7 is less sensitive for detecting change at this early stage.

The percentage change from baseline in the EG eyes is compared with the percentage change in control eyes in Table 2 for each of the SDOCT parameters. The values for percentage change were calculated as the difference between the parameter value at the designated follow-up session and the average of the two baseline values (expressed as a percentage). Table 2 shows that the magnitude of change was generally greater in EG eyes than in control eyes. To evaluate longitudinal changes within each group, we compared the raw parameter values for each eye at each follow-up time point with the average of the two baseline observations for each eye (using paired *t*-tests and a conservative definition of significance, $P < 0.01$). At FU1, four SDOCT parameters were found to have changed significantly from baseline in the EG eyes: mean rim width ($P = 0.003$, paired *t*-test corrected for multiple comparisons), mean rim volume ($P = 0.007$), mean ALCS $\text{depth}_{\text{NCO}}$ ($P = 0.0008$), and mean ALCS depth_{BM} ($P = 0.002$). In EG eyes at FU1, there was no significant change in mean RNFLT ($P = 0.04$) or RNFLV ($P = 0.13$), although both of these parameters declined significantly by FU2 ($P = 0.007$ and $P = 0.009$, respectively). The four parameters identified in EG eyes as having changed significantly at FU1 (mean rim width, rim volume, ALCS $\text{depth}_{\text{NCO}}$, and ALCS depth_{BM}) all continued to have significantly changed from baseline at FU2 ($P = 0.006$, 0.003, 0.001, and 0.0007, respectively). Mean NCO depth relative to peripheral RPE/BM was also found to significantly increase ($P = 0.002$) and mean PLTT to significantly decrease ($P = 0.009$) in EG eyes at FU2. In the control eye group, none of the SDOCT parameters was found to be significantly different from their average baseline ($P > 0.01$) at either follow-up time point.

The identification of change within individual eyes was based on the baseline versus follow-up difference in the parameter of interest exceeding the repeatability coefficient for that parameter. The number of EG and control eyes identified as having changed significantly at FU1 and FU2 are summarized in Table 3. The highest positive hit rate among the EG eyes at FU1 was for ALCS $\text{depth}_{\text{NCO}}$ and ALCS depth_{BM} (both 67%). However, it should be noted that the specificity at FU1 (based on the number of control eyes flagged as changing) was 89% for ALCS $\text{depth}_{\text{NCO}}$ and 78% for ALCS depth_{BM}. Both of the rim parameters (mean rim width and rim volume) did not flag any control eyes as changing at FU1 (equivalent to a specificity of 100%), yet had a positive hit rate of 56% in each case. At FU2, ALCS $\text{depth}_{\text{NCO}}$ and ALCS depth_{BM} had positive hit rates of 78% and 89%, respectively, with no controls flagged as changing (i.e., specificity of 100%); PLTT was flagged as changing in 67% of EG eyes, at FU2, with an estimated specificity of 89%.

An association between the percentage of change in the SDOCT parameter and each method of IOP characterization (mean IOP, peak IOP, and cumulative IOP difference) was observed in the EG eyes at FU2 for each of the parameters. For example, Figure 8 shows the percentage change from baseline to FU2 versus the mean IOP during follow-up in each eye. For each parameter, the group of EG eyes is shown as filled diamonds and the group of control eyes as open circles. Note that the extent of scatter among the control eyes also serves as an indication of total measurement noise against which significant change can be detected for the longitudinal within-eye analysis. Figure 8 shows that there was a significant association between mean IOP and change to FU2 in the following parameters: RNFLT (Fig. 8A, $P = 0.017$, general estimation equation), mean rim width (Fig. 8B, $P = 0.002$), rim volume (Fig. 8C, $P < 0.0001$), ALCS $\text{depth}_{\text{NCO}}$ (Fig. 8D, $P = 0.0008$), ALCS depth_{BM} (Fig. 8E, $P = 0.001$), and PLTT (Fig. 8F, $P = 0.004$).

In the analysis of the percentage of ALCS area marked, there was no significant effect of treatment (EG versus control; $P = 0.80$, RM-ANOVA), no significant effect of time ($P = 0.47$), and no significant interaction between treatment and time ($P = 0.84$). The percentage of ALCS area marked before application of the shared area restriction was 66.6% in control eyes and 66.2% in EG eyes, averaged over all four time points. Interanimal differences accounted for 72% of the overall variance in the percentage of ALCS area marked ($P = 0.0005$). Figure 9 shows the shared ALCS delineation points (i.e., ALCS points present in all four volumes) projected to the NCO for both eyes of all nine animals. While the extent of missing areas is variable between animals, in most eyes they directly correspond to the location of the central retinal vasculature.

An example of the ILM and ALCS displacements seen in EG eyes is illustrated in Figure 10. The changes in this animal represent the approximate midpoint for ONH parameter changes observed in this group of EG eyes at FU2. Note also that these three volumes are aligned in the *Z*-axis by their NCO centroids, thus the ILM and BM/RPE surfaces at the more peripheral portions of the follow-up volumes appear to be displaced anteriorly from baseline; if aligned by their peripheral reference planes, the posterior displacement of the ALCS from baseline would appear to be even greater.

Discussion

This study is the first to describe the application of longitudinal SDOCT imaging to detect deep structural changes in the glaucomatous ONH. Several deep ONH structural parameters were found to change significantly from baseline in eyes with EG and

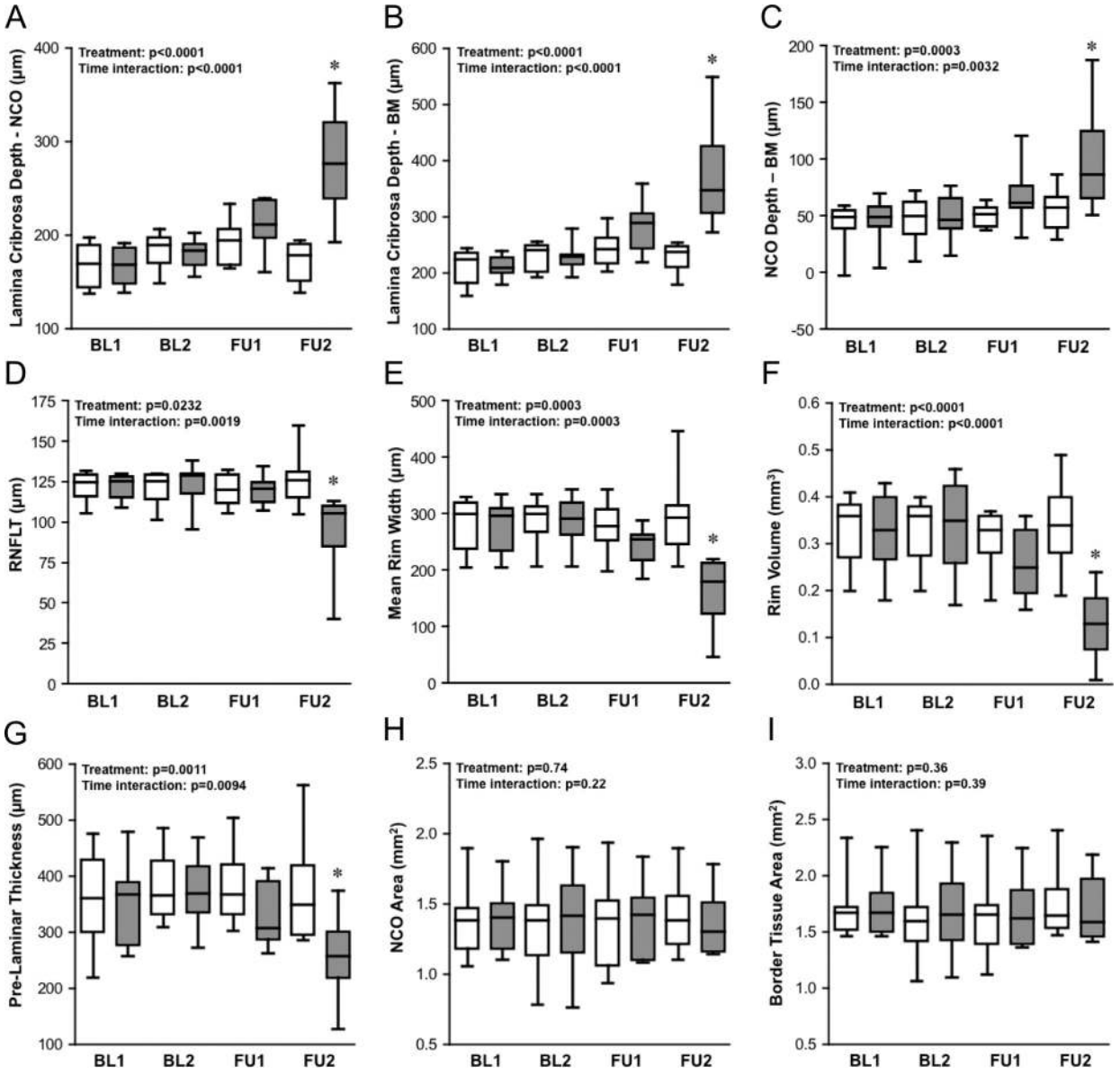

Figure 7. Distribution of parameter values at each time point for the group of EG eyes (*filled boxes*) and the group of control eyes (*open boxes*). Box-and-whisker plots indicate interquartile range (25th–75th percentiles), median (*horizontal line*), lower and upper extremes (*whiskers*). Time points studied are first baseline (BL1), second baseline (BL2), first follow-up (FU1; defined as CSLT onset), and second follow-up (FU2, final data set available for each subject). *Inset*: results of RM-ANOVA with *P* for treatment effect (EG versus control) and treatment–time interaction. *Significant difference between EG and control group at a given time point ($P < 0.001$, Bonferroni corrected post hoc *t*-test).

to remain stable over the same duration in control eyes. The changes were substantial enough at FU2 for the difference to be significant, even by cross-sectional analysis. Importantly, deep ONH structural changes were also found by longitudinal analysis to be present, even at the onset of CSLT-detected ONH surface change. These changes occurred at a stage preceding

Table 2. Percentage Difference between the Average Baseline Parameter Value and the Parameter Value at FU1 and at FU2 for the Group of Control and EG Eyes

	RNFLT	RNFLV	NCO Area	NCO Depth	Border T Area	Rim Width	Rim Volume	PLTT	ALCS $Depth_{NCO}$	ALCS $Depth_{BM}$
Control FU1	−1 (5)	−1 (5)	−1 (9)	6 (18)	−2 (10)	−3 (4)	−4 (8)	3 (9)	10 (14)	11 (13)
EG FU1	−3 (4)	−2 (5)	0 (7)	63 (75)	−1 (5)	−13 (10)	−20 (17)	−8 (9)	24 (15)	28 (20)
P	0.2001	0.3027	0.3380	0.0122	0.4141	0.0138	0.0130	0.0145	0.0720	0.0561
Control FU2	3 (11)	3 (8)	4 (7)	16 (22)	6 (7)	2 (16)	5 (20)	0 (12)	−1 (9)	4 (7)
EG FU2	−23 (22)	−21 (22)	0 (10)	146 (163)	1 (9)	−40 (26)	−56 (30)	−27 (22)	63 (36)	72 (43)
P	0.0181	0.0139	0.0067	0.0109	0.0173	0.0050	0.0011	0.0119	0.0005	0.0008

Data are expressed as the mean percentage. The average baseline value was (BL1 + BL2)/2. *P* values listed represent result of paired *t*-test comparing the change from average baseline in control eyes versus the change from average baseline in EG eyes (significant differences defined at $P < 0.01$).

TABLE 3. Number of Control and EG Eyes Flagged as Changing, Based on the Difference between Baseline and Follow-up Exceeding the Repeatability Coefficient for that Parameter

	RNFLT	RNFLV	NCO Area	NCO Depth	BT Area	Rim Width	Rim Volume	PLTT	ALCS $Depth_{NCO}$	ALCS $Depth_{BM}$
Control FU1	1	1	0	1	1	0	0	0	1	2
Estimated specificity (%)	89	89	100	89	89	100	100	100	89	78
95% CI (%)	56.5–98.0	56.5–98.0	70.1–100.0	56.5–98.0	56.5–98.0	70.1–100.0	70.1–100.0	70.1–100.0	56.5–98.0	45.3–93.7
Control FU2	1	1	0	2	0	1	2	1	0	0
Estimated specificity (%)	89	89	100	78	100	89	78	89	100	100
95% CI (%)	56.5–98.0	56.5–98.0	70.1–100.0	45.3–93.7	70.1–100.0	56.5–98.0	45.3–93.7	56.5–98	70.1–100.0	70.1–100.0
EG FU1	0	0	0	2	0	5	5	0	6	6
Positive hit rate (%)	0	0	0	22	0	56	56	0	67	67
95% CI (%)	0.0–29.9	0.0–29.9	0.0–29.9	6.3–54.7	0.0–29.9	26.7–81.1	26.7–81.1	0.0–29.9	35.4–87.9	35.4–87.9
P	0.1517	0.1517	NA	0.2635	0.1517	0.0043	0.0043	NA	0.0078	0.0289
EG FU2	6	5	0	6	0	8	7	6	7	8
Positive hit rate (%)	67	56	0	67	0	89	78	67	78	89
95% CI (%)	35.4–87.9	26.7–81.1	0.0–29.9	35.4–87.9	0.0–29.9	56.5–98.0	45.3–93.7	35.4–87.9	45.3–93.7	56.5–98.0
P	0.0078	0.0228	NA	0.0289	NA	0.0005	0.0092	0.0078	0.0004	0.0001

The 95% CI is listed under each proportion. The *P* values listed represent the result of a Z-test for two proportions comparing the positive hit rate for the treated eye group with that for the control eye group at each of the follow-up time points. Estimated specificity: (number of control eyes not changing/total control eyes) × 100; positive hit rate: (number of EG eyes changing/total EG eyes) × 100.

loss of neural tissue as measured by two parameters, peripapillary RNFLT and RNFLV. Changes in the neuroretinal rim parameters (rim width and rim volume) were, however, detectable at the onset of surface height depression. A possible explanation as to why this may occur is that some of the changes occurring at the rim at the earliest time point may reflect conformational changes in the neural and nonneuronal components of the rim that follow deformation of the underlying and adjacent connective tissues. By contrast, a greater proportion of the changes detected at the more eccentric peripapillary RNFL will likely reflect true loss of axonal tissue, rather than conformational changes in connective tissues. This finding underscores important potential advantages of SDOCT imaging. Specifically, deep ONH changes are detectable at a very early stage (at least in this experimental model of glaucoma) and are distinct from the axonal loss reflected by RNFL thinning. These deep ONH changes underlie the early ONH surface height changes detected by CSLT.

The use of RNFLT measurements as captured by TDOCT is generally well established in glaucoma patients.[19–22] This validation comes with the caveat, however, that there is a relative paucity of published reports of longitudinal RNFL measurements in human subjects.[4,5] While we demonstrated, as expected, that RNFL thinning was detectable at FU2 in this experimental model, we were also successful in demonstrating the principal goal of this study. Specifically, this was to explore the potential for detecting changes in deep, subsurface ONH structures (at the prelaminar and laminar level) by longitudinal SDOCT imaging. It has recently been suggested, albeit in a cross-sectional study, that SDOCT can detect thinning of the lamina in a series of ocular hypertensive and glaucomatous eyes and that this thinning correlates with a reduction in visual field mean defect.[10] We were unable to replicate this finding in the present study as we could not reliably detect the full thickness of the lamina in all images.

The results of this study also demonstrated, at least in the sample of EG eyes examined in this study, that progressive glaucomatous changes include reduction of the PLTT, posterior displacement of the ALCS and NCO, and decline of the rim parameters (mean rim width and rim volume). Of note, these deep ONH changes were detectable before the onset of peripapillary RNFL thinning at FU1, at the onset of HRT-detected surface topography depression. Additional studies are under way to evaluate what deep ONH changes can be detected by SDOCT before surface height depression. Interestingly, a recent study has demonstrated that TCA changes may precede the onset of visual field changes as measured using the Early Manifest Glaucoma Treatment Trial perimetric criteria.[23] It is likely that surface height changes at the onset detectable by HRT are generated by a combination of changes beneath the ONH surface, such as posterior laminar displacement and changes in the shape of the scleral canal and/or posterior eye wall, the latter being inferred from the changes in NCO depth relative to peripheral BM reference plane. One cannot, therefore, assume that TCA change can isolate either prelaminar changes or laminar displacement alone. Given that surface height depression is specifically designed to detect changes within the nerve head, there is a potential bias against detection of change in the peripapillary RNFL. Given that our structural endpoint was based on the HRT and this device does not measure the RNFL directly, it would have been improper to use this as our structural endpoint. As OCT (whether time domain or spectral domain) has a well-established utility for detecting RNFL changes, any changes in RNFL parameters occurring at the onset of surface height depression should have been detected.

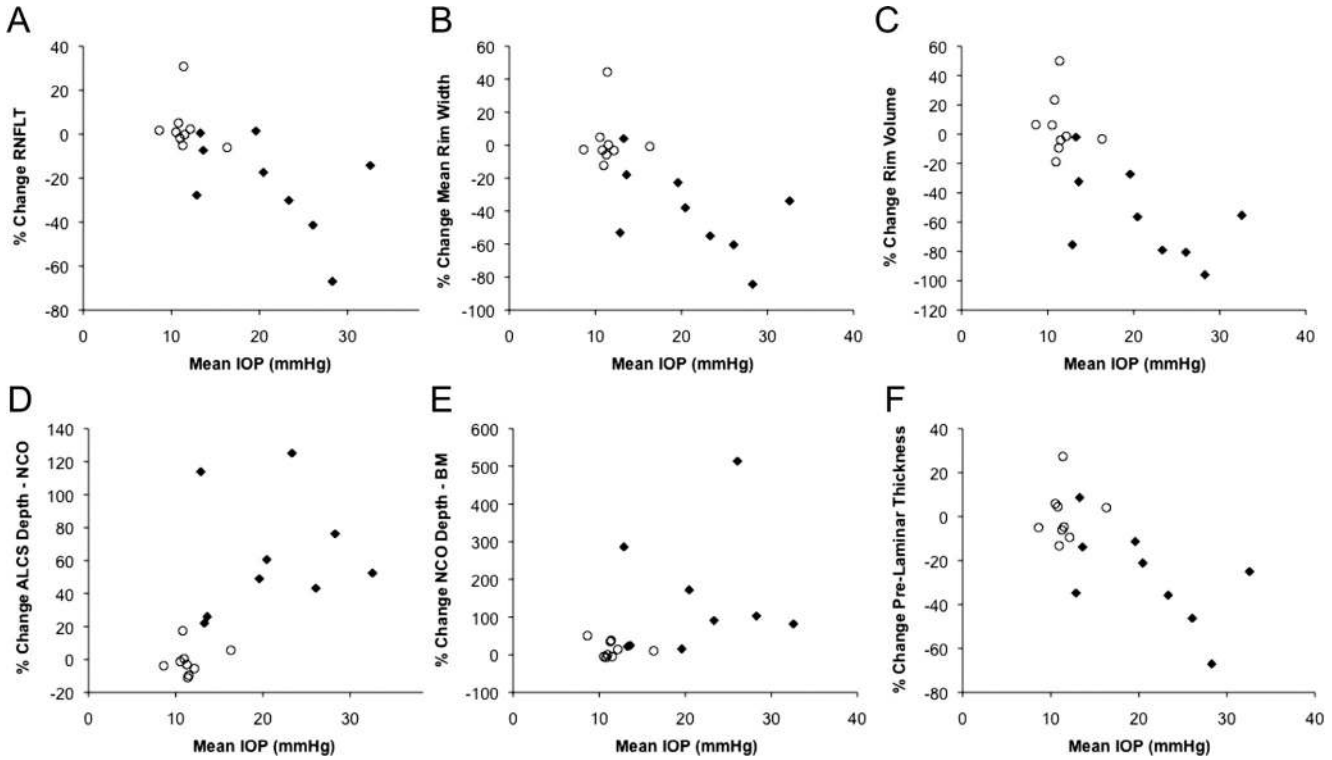

FIGURE 8. The relationship between mean IOP and change in the magnitude of SDOCT parameter (mean baseline value; FU2 value). (♦) Experimental glaucoma eyes; (○) control eyes.

In addition to the changes in the PLTT and ALCS, the rim parameters derived from SDOCT volumes proved to be robust and sensitive.

Povazy et al.[24] have described a method known as minimum distance mapping that identifies thinning of the circumpapillary nerve fiber band in glaucomatous eyes. Our approach for measuring mean rim width used a very similar technique, although we took our measurements from the NCO. Povazy et al. also used the termination of the RPE signal but suggested that this landmark was equivalent to the scleral ring of Elschnig and the termination of the sclera. Our examination of the clinical disc margin in 3D histomorphometric reconstructed nerves and in 3D SDOCT ONH volumes indicate that this is not the case, with the NCO, BT of Elschnig (the correct anatomic landmark for Elschnig's ring), and the anterior scleral canal opening each being detectable as separate structures and each potentially constituting the disc margin, even within the same nerve.[16,25] SDOCT-detected loss of neuroretinal rim is an important finding as rim loss has a clear relation to what occurs in clinical glaucoma. This feature has been exploited both in HRT classification systems and HRT progression algorithms.[3,26,27]

Given the similarity between the experimental optic neuropathy and human glaucomatous optic neuropathy and the fact that a commercially available imaging device was used, it is reasonable to assume that the findings of this study will be applicable to human patients and are likely to be replicated in studies of human subjects. There are, however, several important caveats to take into consideration when trying to translate these findings into clinical practice. First, this study was intended as a test of the hypothesis that deep ONH changes could be detected by longitudinal SDOCT imaging. In general, a progression algorithm of this type (an event analysis) will need to be more robust in practice, as clinical management decisions may well be based on the observed changes. The most direct way of increasing specificity in a clinical setting would be to perform additional confirmatory tests. However, for the purposes of this study, the choice of an event analysis was preferable for detecting parameter change given the limited number of data-points selected. Our intention was to evaluate whether detection of deep ONH changes was feasible by SDOCT. Given that our results suggest that this is the case, there is now scope for us to expand our longitudinal studies to include additional time points in the development of a more refined progression algorithm. Indeed, future studies will consider both finer spatial and temporal resolution, such that a larger number of time points in longitudinal series will be evaluated and sectoral ONH parameters will be analyzed. The inclusion of an expanded number of time points will allow development of a trend analysis, with the advantages of being able to monitor parameter behavior over time and to generate measures of rate of change. However, development of reliable automated segmentation algorithms is necessary, to improve clinical implementation of any such detection algorithms.

In a previous report by our group, based on postmortem 3D ONH histomorphometric reconstructions, significant prelaminar tissue thickening was identified at the earliest stages of the experimental neuropathy (at a stage equivalent, but not identical with, FU1 in the present study).[8] By contrast, this was not seen in the EG eyes imaged in vivo by SDOCT in the present study. It is possible that there are regional changes in which prelaminar tissue thickening is evident at FU1 and masked by prelaminar tissue thinning in other regions of the same ONH. To confirm whether or not this finding is present in vivo using longitudinal SDOCT imaging, a more detailed examination (both globally and regionally) of sequential volumes, up to and beyond the detection of HRT surface height depression, will be required. Such an examination is beyond the scope of the present study, but is being undertaken in another study in progress. It is also possible that the histomorphometric evidence of prelaminar tissue thickening in our previous report was the result of an interaction between the ONH tissues of experimental eyes and the histologic processing that did not

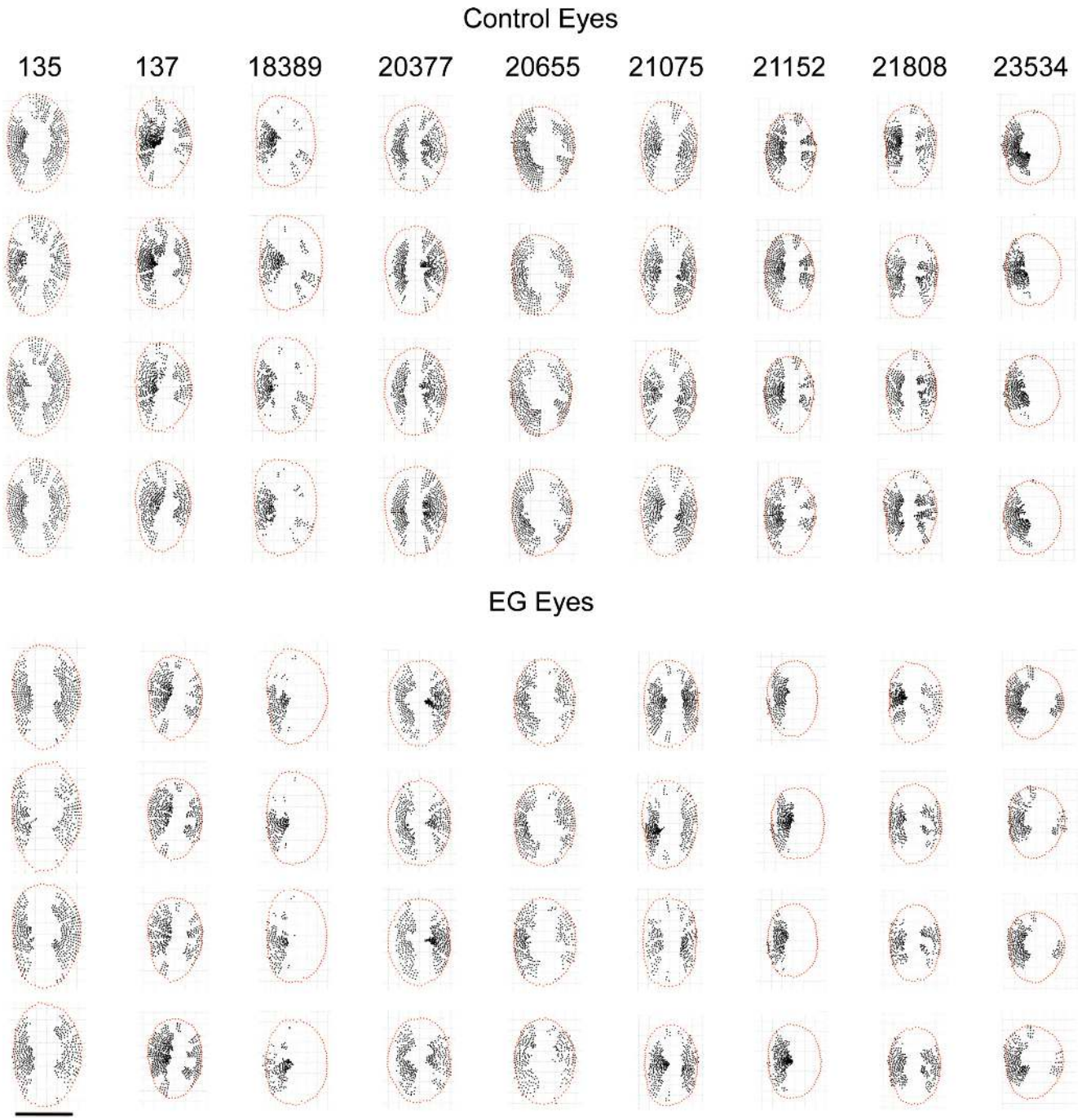

FIGURE 9. Longitudinally shared, SDOCT-detected ALCS points. ALCS points (*black points*) are projected to the NCO reference plane (*red points*); all eyes are in the right eye orientation. Calibration bar, 1 mm.

occur in the contralateral normal eyes, which were processed identically. This possibility will also be explored in the study that is in progress.

The degree of ALCS and ILM displacement observed in this study may well exceed that which might be expected in human subjects, given that the peak IOPs recorded in the EG eyes (range, 23.7–61.0 mm Hg at FU2) likely exceed those recorded in human ocular hypertensive or treated glaucoma subjects. By stabilizing the IOP at 10 mm Hg at each imaging session, we took measures to ensure that the structural changes observed by SDOCT were the result of cumulative damage and not secondary to an increased level of IOP at the time of imaging. Indeed, acute IOP elevation has been reported to cause similar changes in the shape of the ONH and peripapillary structures.[15] Overall, the mean IOPs for the EG eyes were within the range observed clinically in glaucoma patients (range, 14.4–31.9 mm Hg at FU2), but there was clearly a wide variation in results across tests. Even so, it is interesting to note that at least half of the EG eyes at FU1 (at the onset of HRT surface height depression) had a minimal cumulative IOP insult (i.e., all IOP measurements in some EG eyes had been similar to those recorded in their fellow control eyes up to that follow-up time point). There was, however, a clear association between parameter changes and magnitude of IOP (whether mean, peak, or cumulative insult) in the EG eyes. Our IOP characterization in these animals is limited to approximately weekly measurements,

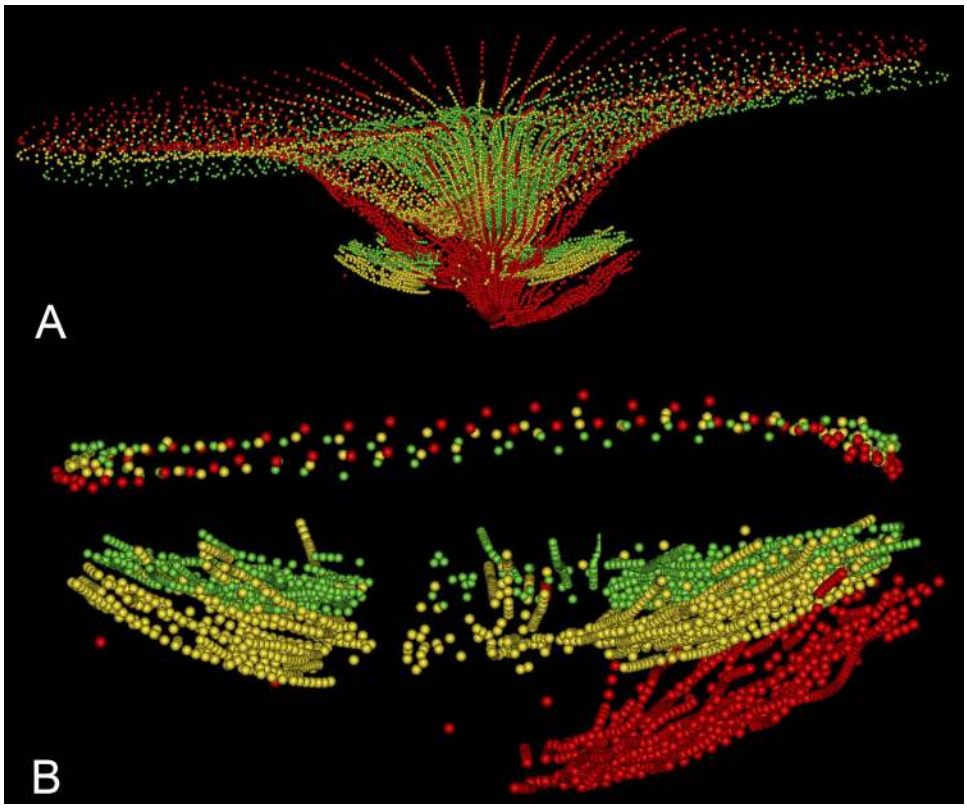

FIGURE 10. ILM and ALCS displacement in an EG eye (18389 in Fig. 9). (**A**) ILM and ALCS delineations are shown, with BL1 (*green*), FU1 (*yellow*) and FU2 (*red*). (**B**) The ALCS delineations are magnified, anchored at the level of the NCO (shown above the ALCS delineations).

but we have no record of the IOPs between these dates. These issues will be addressed by real-time IOP telemetry. We are currently trialing implantable intraocular IOP telemetry devices in a number of normal monkey eyes in collaboration with the Devers Ocular Biomechanics Laboratory.

We have previously suggested that the Bruch's membrane opening or NCO would serve as an optimal, stable, zero-reference plane in both our 3D histomorphometric reconstructions and in 3D SDOCT ONH volumes.[7,9,14] We therefore adopted an NCO-based reference plane as the primary reference plane for our quantification in this study. However, we have previously reported evidence that the ONH likely deforms outward relative to the peripheral retina after acute IOP elevations.[28] The results of the present study demonstrate posterior movement of the NCO relative to the peripheral Bruch's membrane in the setting of chronic IOP elevation and confirm previous 3D histomorphometric detection of this finding at the earliest stages of the neuropathy (in this study at FU1).[9,29] Peripheral Bruch's membrane is assumed to be relatively stable in the neuropathy.

The above findings do not necessarily preclude the use of the NCO as the basis for an SDOCT reference plane. First, it is reasonable to expect that an NCO reference plane is valid for the quantification of ONH parameters that are bound within the NCO circumference. Although the entire ONH (including the NCO) may move posteriorly (relative to the more peripheral Bruch's membrane) with progressive neuropathy, the structures within the nerve head will still be displaced relative to the NCO. This displacement is demonstrated by the fact that the relative degree of posterior displacement of the ALCS was similar regardless of whether the peripheral Bruch's membrane or NCO reference plane was used. Second, the NCO is still required for the generation of the peripheral Bruch's membrane reference plane in our current scheme, as it is anchored to the NCO centroid. The NCO is likely to be a relatively simple target for automatic segmentation algorithms, so it will be a key landmark in the definition of reference planes, whether centrally or peripherally located. Moreover, the NCO area did not change significantly in any of the eyes (EG or control eyes) at any time point, thus the NCO centroid should serve as a relatively stable reference.

A peripheral reference plane will be vital for structures external to the NCO area, such as the peripapillary sclera. We were unable to reliably detect peripapillary sclera in the monkey eyes examined in this study but have noted in our preliminary SDOCT examinations of human eyes that the scleral surface may be more easily detected in myopic and glaucomatous human eyes. We have identified expansion of the scleral canal opening as an important histomorphometric finding in early EG.[9] We therefore fully expect that parameters based on the detection of the peripapillary sclera will become important, which will necessitate the use of a peripheral, NCO-anchored, reference plane. The adoption of a longer wavelength ($\sim$1 μm) SDOCT imaging source may result in improved detection of deeper ONH structures, including the scleral architecture.[24,30,31] We are soon to begin testing of a prototype device (Spectralis; Heidelberg Engineering) outfitted with a 1060 nm center-wavelength imaging source; a comparison with existing 870 nm wavelength technology will be pursued as part of our preliminary assessments. An alternative method, not used in the present study, which has been reported to improve depth penetration, involves advancing the SDOCT imaging head anteriorly so that the fundus image is inverted.[32]

There are several issues concerning the detection of the ALCS in the SDOCT volumes examined in this study. It is clear that detection of the ALCS is frequently incomplete, particularly in regions where there is shadowing from the central retinal vasculature. It is unclear whether the observer's ability to detect the anterior lamina was influenced by the thickness of prelaminar tissue. One may hypothesize that the degree of ALCS detection increases as glaucoma progresses, as depth

penetration improves with the diminution of the prelaminar tissue. It is equally plausible that the detection of the ALCS may improve because changes in the conformation of lamina architecture and/or its tissue properties as glaucoma progresses may strengthen the reflectance signal. However, our examination of the percentage of ALCS regions marked across the four volumes for each of the nine eyes suggests that a relatively large proportion (approximately two thirds of the laminar area on average) was detected and reproducibly delineated and that the area of ALCS marked was reliable over time in both control and EG eyes. The rationale for choosing two or more ALCS points in each of the 100 subdivisions to be the minimal threshold for detection across the four images was to balance a desire to limit spurious detection of ALCS (as may occur with a single ALCS point in a region), while not being so conservative as to exclude genuine ALCS delineations (by not filtering out regions with greater than two ALCS points). At present, automatic segmentation of the lamina is likely to be very difficult, as it is so highly variable. By meticulously comparing serial histologic sections of a normal monkey ONH with matched B-scans acquired by SDOCT from the same eye,[17] we have been able to establish visual clues that are indicative of the ALCS in an SDOCT volume. The masked observers were trained to recognize the same features of the ALCS signal (using a different data set). We minimized the impact of interobserver reproducibility by factoring it into the study design (control eyes) as well as into the progression algorithm used to flag individual eyes as progressing given that any parameter change in any individual eye had to exceed the RC for that parameter.

There remains a potential concern that some of the structural changes we believe are being detected by SDOCT may be due to an acute IOP effect, rather than to a chronic IOP cumulative insult. In other words, some acute IOP-related ONH deformation may remain despite 30 minutes of IOP stabilization at 10 mm Hg. Our previous assessments of EG eyes, both by conventional serial histology and by 3D histomorphometric reconstruction, with exactly the same level of EG damage (at the onset of repeatable surface height depression) would indicate that the profound alterations in ONH structure are genuine and the effect of acute IOP on these changes is negligible after 30 minutes of IOP stabilization.[7–9,12,28,29,33,34] Furthermore, the changes that we propose are detectable by SDOCT imaging are likely to represent changes caused by tissue remodeling, rather than just by an acute deformation.[35] We are continuing to explore this phenomenon by studying the effect of acute IOP elevation on each of the parameters generated in this study in a series of normal monkey eyes.

In summary, in this study we report SDOCT-detected ONH changes in longitudinally examined eyes with EG optic neuropathy. This SDOCT imaging study is the first to report longitudinal changes at the level of prelaminar and laminar tissues. The results of the study support the ability of SDOCT imaging to detect ONH structural damage in human subjects with, or at risk of, glaucoma. The prelaminar tissue thickness and anterior laminar surface height are tangible targets for human imaging. Further study is needed to establish robust, specific progression algorithms and to identify what constitutes clinically important changes in these structures.

Acknowledgments

The authors thank Lin Wang for allowing his animal subjects to be incorporated into this study.

References

1. Artes PH, Chauhan BC. Longitudinal changes in the visual field and optic disc in glaucoma. *Prog Retin Eye Res.* 2005;24:333–354.
2. Chauhan BC, Hutchison DM, Artes PH, et al. Optic disc progression in glaucoma: comparison of confocal scanning laser tomography to optic disc photographs in a prospective study. *Invest Ophthalmol Vis Sci.* 2009;50:1682–1691.
3. Fayers T, Strouthidis NG, Garway-Heath DF. Monitoring glaucomatous progression using a novel Heidelberg Retina Tomograph event analysis. *Ophthalmology.* 2007;114:1973–1980.
4. Wollstein G, Schuman JS, Price LL, et al. Optical coherence tomography longitudinal evaluation of retinal nerve fiber layer thickness in glaucoma. *Arch Ophthalmol.* 2005;123:464–470.
5. Medeiros FA, Zangwill LM, Alencar LM, et al. Detection of glaucoma progression with stratus OCT retinal nerve fiber layer, optic nerve head, and macular thickness measurements. *Invest Ophthalmol Vis Sci.* 2009;50:5741–5748.
6. Alencar LM, Zangwill LM, Weinreb RN, et al. Agreement for detecting glaucoma progression with the GDx guided progression analysis, automated perimetry, and optic disc photography. *Ophthalmology.* 2010;117:462–470.
7. Downs JC, Yang H, Girkin C, et al. Three dimensional histomorphometry of the normal and early glaucomatous monkey optic nerve head: neural canal and subarachnoid space architecture. *Invest Ophthalmol Vis Sci.* 2007;48:3195–3208.
8. Yang H, Downs JC, Bellezza AJ, Thompson H, Burgoyne CF. 3-D Histomorphometry of the normal and early glaucomatous monkey optic nerve head: prelaminar neural tissues and cupping. *Invest Ophthalmol Vis Sci.* 2007;48:5068–5084.
9. Yang H, Downs JC, Girkin C, et al. 3-D histomorphometry of the normal and early glaucomatous monkey optic nerve head: lamina cribrosa and peripapillary scleral position and thickness. *Invest Ophthalmol Vis Sci.* 2007;48:4597–4607.
10. Inoue R, Hangai M, Kotera Y, et al. Three-dimensional high-speed optical coherence tomography imaging of lamina cribrosa in glaucoma. *Ophthalmology.* 2009;116:214–222.
11. Burgoyne CF, Varma R, Quigley HA, Vitale S, Pease ME, Lenane PL. Global and regional detection of induced optic disc change by digitized image analysis. *Arch Ophthalmol.* 1994;112:261–268.
12. Burgoyne CF, Downs JC, Bellezza AJ, Hart RT. Three-dimensional reconstruction of normal and early glaucoma monkey optic nerve head connective tissues. *Invest Ophthalmol Vis Sci.* 2004;45:4388–4399.
13. Chauhan BC, Blanchard JW, Hamilton DC, LeBlanc RP. Technique for detecting serial topographic changes in optic disc and peripapillary retina using scanning laser tomography. *Invest Ophthalmol Vis Sci.* 2000;41:775–782.
14. Strouthidis NG, Yang H, Fortune B, Downs JC, Burgoyne CF. Detection of optic nerve head neural canal opening within histomorphometric and spectral domain optical coherence tomography data sets. *Invest Ophthalmol Vis Sci.* 2009;50:214–223.
15. Fortune B, Yang H, Strouthidis NG, et al. The effect of acute intraocular pressure elevation on peripapillary retinal thickness, retinal nerve fiber layer thickness, and retardance. *Invest Ophthalmol Vis Sci.* 2009;50:4719–4726.
16. Strouthidis NG, Yang H, Reynaud JF, et al. Comparison of clinical and spectral domain optical coherence tomography optic disc margin anatomy. *Invest Ophthalmol Vis Sci.* 2009;50:4709–4718.
17. Strouthidis NG, Grimm J, Williams GA, Cull GA, Wilson DJ, Burgoyne CF. A comparison of optic nerve head morphology viewed by spectral domain optical coherence tomography and by serial histology. *Invest Ophthalmol Vis Sci.* 2010;51:1464–1474.
18. Bland JM, Altman DG. Statistical methods for assessing agreement between two methods of clinical measurement. *Lancet.* 1986;1:307–310.
19. Medeiros FA, Zangwill LM, Bowd C, Vessani RM, Susanna R Jr, Weinreb RN. Evaluation of retinal nerve fiber layer, optic nerve head, and macular thickness measurements for glaucoma detection using optical coherence tomography. *Am J Ophthalmol.* 2005;139:44–55.
20. Deleon-Ortega JE, Arthur SN, McGwin G Jr, Xie A, Monheit BE, Girkin CA. Discrimination between glaucomatous and nonglaucomatous eyes using quantitative imaging devices and subjective optic nerve head assessment. *Invest Ophthalmol Vis Sci.* 2006;47:3374–3380.

21. Schuman JS, Hee MR, Puliafito CA, et al. Quantification of nerve fiber layer thickness in normal and glaucomatous eyes using optical coherence tomography. *Arch Ophthalmol.* 1995;113:586–596.
22. Bowd C, Weinreb RN, Williams JM, Zangwill LM. The retinal nerve fiber layer thickness in ocular hypertensive, normal, and glaucomatous eyes with optical coherence tomography. *Arch Ophthalmol.* 2000;118:22–26.
23. Chauhan BC, Nicolela MT, Artes PH. Incidence and rates of visual field progression after longitudinally measured optic disc change in glaucoma. *Ophthalmology.* 2009;116:2110–2118.
24. Povazay B, Hofer B, Hermann B, et al. Minimum distance mapping using three-dimensional optical coherence tomography for glaucoma diagnosis. *J Biomed Opt.* 2007;12:041204.
25. Strouthidis NG, Yang H, Downs JC, Burgoyne CF. Comparison of clinical and three-dimensional histomorphometric optic disc margin anatomy. *Invest Ophthalmol Vis Sci.* 2009;50:2165–2174.
26. Wollstein G, Garway-Heath DF, Hitchings RA. Identification of early glaucoma cases with the scanning laser ophthalmoscope. *Ophthalmology.* 1998;105:1557–1563.
27. Strouthidis NG, Scott A, Peter NM, Garway-Heath DF. Optic disc and visual field progression in ocular hypertensive subjects: detection rates, specificity, and agreement. *Invest Ophthalmol Vis Sci.* 2006;47:2904–2910.
28. Yang H, Downs JC, Sigal IA, Roberts MD, Thompson H, Burgoyne CF. Deformation of the normal monkey optic nerve head connective tissue after acute IOP elevation within 3-D histomorphometric reconstructions. *Invest Ophthalmol Vis Sci.* 2009;50:5785–5799.
29. Yang H, Downs JC, Burgoyne CF. Physiologic intereye differences in monkey optic nerve head architecture and their relation to changes in early experimental glaucoma. *Invest Ophthalmol Vis Sci.* 2009;50:224–234.
30. Povazay B, Hermann B, Unterhuber A, et al. Three-dimensional optical coherence tomography at 1050 nm versus 800 nm in retinal pathologies: enhanced performance and choroidal penetration in cataract patients. *J Biomed Opt.* 2007;12:041211.
31. Srinivasan VJ, Adler DC, Chen Y, et al. Ultrahigh-speed optical coherence tomography for three-dimensional and en face imaging of the retina and optic nerve head. *Invest Ophthalmol Vis Sci.* 2008;49:5103–5110.
32. Spaide RF, Koizumi H, Pozzoni MC. Enhanced depth imaging spectral-domain optical coherence tomography. *Am J Ophthalmol.* 2008;146:496–500.
33. Bellezza AJ, Rintalan CJ, Thompson HW, Downs JC, Hart RT, Burgoyne CF. Deformation of the lamina cribrosa and anterior scleral canal wall in early experimental glaucoma. *Invest Ophthalmol Vis Sci.* 2003;44:623–637.
34. Yang H, Thompson H, Roberts MD, Sigal IA, Downs JC, Burgoyne CF. Deformation of the early glaucomatous monkey optic nerve head connective tissue following acute IOP elevation within 3-D histomorphometric reconstructions. *Invest Ophthalmol Vis Sci.* 2011;52:345–363.
35. Roberts MD, Grau V, Grimm J, et al. Remodeling of the connective tissue microarchitecture of the lamina cribrosa in early experimental glaucoma. *Invest Ophthalmol Vis Sci.* 2009;50:681–690.